Mechanical response of holographic photopolymers

Amy C. Sullivan, Shankar Lalitha Sridhar, Amy Resman, David J. Glugla, Marvin D. Alim, et al.

Amy C. Sullivan, Shankar Lalitha Sridhar, Amy Resman, David J. Glugla, Marvin D. Alim, Franck Vernerey, Robert R. McLeod, "Mechanical response of holographic photopolymers," Proc. SPIE 10233, Holography: Advances and Modern Trends V, 102330O (15 May 2017); doi: 10.1117/12.2265878

SPIE.

Event: SPIE Optics + Optoelectronics, 2017, Prague, Czech Republic

Mechanical Response of Holographic Photopolymers

Amy C. Sullivan[a], Shankar Lalitha Sridhar[b], Amy Resman[c], David J. Glugla[a], Marvin D. Alim[d], Franck Vernerey[b], Robert R. Mcleod[a]

[a]Department of Electrical Engineering, 425 UCB, Boulder, CO USA 80309; [b]Department of Mechanical Engineering, 427 UCB, Boulder, CO USA 80309; [c]Department of Chemical and Biological Engineering, 596 UCB, Boulder, CO USA 80309; [d]Material Science and Engineering Program, University of Colorado, 596 UCB, Boulder, CO USA 80309

ABSTRACT

Two-chemistry polymer systems are attractive platforms for a wide range of optical and mechanical applications due to the orthogonal chemistries of the initial thermoset matrix and the subsequent photo-initiated polymerization. This scheme allows the mechanical and optical properties of the materials to be individually addressed. However, the mechanical properties of both the initial matrix and the photopolymer system affect the performance of these materials in many applications from holography to optically-actuated folding. We present a mechanical model along with experimental demonstrations of a two-chemistry holographic photopolymer system. A three-dimensional finite element model is used to simulate the mechanical and chemical responses in time. The model uses standard material measurements to predict both large-scale deformation and more localized stress and strain. To demonstrate the magnitude of mechanical stresses possible in these materials, we show bending of thin strips with UV light activation using an optical absorber to create an intensity gradient in depth. The resulting non-uniform polymerization causes shrinkage and bending toward the light followed by swelling and bending away from the light caused by monomer diffusion. In addition to this large-scale bending, we demonstrate that the model can be used to qualitatively predict surface deformations that can be used for surface relief optical elements. The mechanical model enables understanding of shrinkage and swelling properties of a material system that affect the performance of that system over a wide range of illumination conditions.

Keywords: photopolymer, mechanical model, origami, surface relief gratings, holography

1. INTRODUCTION

High quality holograms, desirable for high diffraction efficiency holographic optical elements [1,2], require not only high refractive index changes, but also control over the shrinkage and mechanical stability of the materials during recording. In many two-chemistry polymer systems used for holography, there is an initial thermoset matrix that sets the mechanical properties of the material. Then, a smaller percentage of the mixture is devoted to a high index of refraction molecule that is photo-initiated. Upon localized light initiation and subsequent polymerization, an area of low monomer concentration is created where the light illuminates the sample. This concentration gradient causes diffusion of the mobile monomer species into the bright areas. Diffusion of monomer in holographic materials can cause significant mechanical stresses, especially as concentration of high index species increases to obtain large refractive index change.

While bulk shrinkage in holographic photopolymers has been studied extensively [3,4,5], local mechanical stresses have received less attention. These mechanical stresses that occur through the diffusion of monomer can cause non-uniformity in holograms, decreasing peak diffraction efficiency and affecting the angular Bragg selectivity, as well as stress birefringence, surface relief elements in unconstrained films, and even large scale bending in some circumstances. We investigate a model material with large mechanical stress to demonstrate a mechanical model of the material that can be applied to other two-chemistry photopolymers, different geometries and optical patterning systems. Understanding the large scale mechanical deformations can help develop an intuition for the stresses happening on smaller scales.

To demonstrate the magnitude of the mechanical stress, we demonstrate bending of thin strips in this two-chemistry photopolymer system with ultraviolet (UV) light activation. An optical absorber is added to create an intensity profile that decreases in depth. The UV light initiates photopolymerization in the bright areas, causing an initial shrinkage and bending of the film toward the light. The monomer concentration gradient results in diffusion of monomer from the dark areas to the bright areas, causing swelling. The swelling results in bending of the film away from the light. We achieve

Holography: Advances and Modern Trends V, edited by Miroslav Hrabovský, John T. Sheridan, Antonio Fimia,
Proc. of SPIE Vol. 10233, 102330O · © 2017 SPIE · CCC code: 0277-786X/17/$18 · doi: 10.1117/12.2265878

bending of 120 μm thick films, with radii of curvature as small as 1 mm in less than 2 hours with a single optical exposure and no post processing.

In addition to this large-scale bending, we demonstrate that the model can be used to qualitatively predict surface deformations that have been observed to become a significant issue in open or unconstrained film processing, especially at large spatial frequencies [6,7,8]. We create surface relief gratings using a mask illumination and show how the surface height scales with pitch spacing of the grating. Understanding the formation of these gratings will not only help prevent unwanted surface features in volume holograms, but also improve design of surface optical elements. This will allow for better design of materials and optical exposures to control the final optical and mechanical properties of devices such as holographic optical elements.

2. MATERIAL CHARACTERIZATION

2.1 Materials fabrication

The "liquid" components of the photopolymer gel commonly include a photoinitiator and monomer encapsulated within a solid, crosslinked polymer network via an orthogonal polymerization reaction. Light exposure initiates polymerization, locally consuming the monomer and creating immobile polymer chains. Subsequent diffusion causes the monomer concentration to re-equilibrate, after which a final uniform light exposure polymerizes the remaining monomer and renders the material optically inert. The resulting material has higher concentration of photopolymer and lower concentration of cross-linked network in regions of optical exposure, leading to refractive index approximately equal to the volume fraction weighted average of the refractive indices of the two components.

The crosslinked matrix of the two-component photopolymer system consists of a stoichiometric ratio of polyisocyanate (Desmodur N3900, Covestro AG) and polyol (polycaprolactone-block-polytetrahydrofuran-block-polycaprolactone, Sigma Aldrich) that forms a flexible polyurethane. The photoreactive component contains of a 1:10 molar ratio of photoinitiator TPO (2, 4, 6-Trimethylbenzoyl-diphenyl-phosphineoxide, Sigma Aldrich) and commercially purchased trimethylolpropane ethoxylate triacrylate (TMPTA, Sigma Aldrich), a trifunctional acrylate. Samples were made with 20 wt% of this writing monomer. The matrix and photoreactive components were mixed together in their liquid form at 60°C, degassed, and then cast between two 1 mm glass microscope slides. Sample thicknesses were set using polyester spacers ranging between 100 to 500 μm. Matrix polymerization occurred via the isocyanate reaction overnight in an oven at 60°C. Additionally, samples used for bending experiments contained 0.5 wt% of a ultraviolet optical absorber (Tinuvin 328, Ciba Specialty Chemicals) to provide a gradient in light intensity through the thickness of the sample.

2.2 Materials measurements

A number of materials parameters are used to inform the mechanical model and move toward a quantitative picture of the stress and strain in the material. Information on the modulus of the material before and after cure, the volume changes from swelling in monomer, the diffusion and polymerization times, and shrinkage all affect how the material with bend and deform under optical illumination.

Compressive strain tests were performed on a mechanical test system (MTS Systems Corporation) between two parallel plates using 250 N and 1000 N load cells to determine the polymer compressive modulus. The compressive modulus was taken to be the slope of the polymer stress-strain curve at 15% strain. Tests were performed on three sets of samples: polyurethane matrix only, polyurethane matrix with 20 wt% writing monomer before light illumination and polyurethane matrix with 20 wt% monomer after full optical cure. The initial modulus for just the urethane matrix with no writing monomer was found to be 3 MPa. When the matrix is set up with 20 wt% monomer mixed into the solution, the compressive modulus decreases by a factor of 2 to 1.5 MPa. After fully curing the writing monomer with a 365 nm light source, this modulus increases significantly to 20 MPa, likely due to the additional highly crosslinked network formed by the tri-functional acrylate writing system.

The volume change in the urethane matrix caused by in-diffusion of additional acrylate monomer is another factor affecting the strain of the samples under light illumination. Samples of matrix with no writing monomer were formed into ~ 280 μm thick, 2.5 mm x 13 mm thin strips. The weight and spatial dimensions of the strips were measured, and then the samples were immersed in the liquid TMPTA monomer for varying amounts of time. The samples were then removed, allowed to equilibrate and re-measured. The results of the swelling are shown in Figure 1.

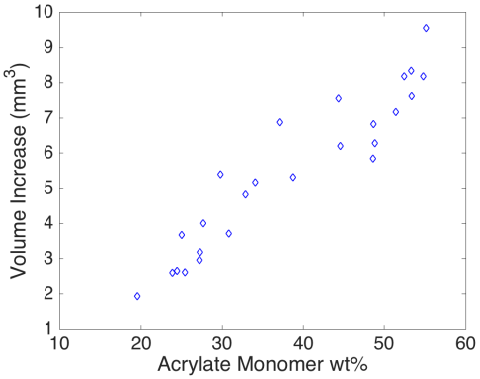

Figure 1. Swelling results. Samples were immersed into triacrylate monomer and the volume increase of each sample was measured and plotted vs. the wt% of monomer which had diffused into it.

The index change and mechanical deformations are caused by diffusion of the mobile acrylate monomers through the urethane matrix. This characteristic diffusion time, especially when compared to the polymerization rate, is essential for modeling the mechanical response of the material. Diffusion was measured by allowing the liquid acrylate monomer to diffuse into 500 μm thick sheets of the urethane matrix and measuring the concentration of acrylate monomer in the samples as a function of time. The data was fit to a model for diffusion into an infinite plane sheet [9], an assumption which is valid for these thin films. The diffusion constant for diffusion of the monomer into the matrix is 1.0 +/- 0.1 $\mu m^2/s$. Once the writing monomer is polymerized, we know from our compressive tests that the modulus of the material changes significantly and so we expect the diffusion coefficient to decrease. Additional tests were performed on strips of the urethane matrix containing 20 wt% of the acrylate monomer that had been fully polymerized with a 365 nm light source. The data for this test is shown in Figure 2 and demonstrates the decrease in diffusivity with a diffusion constant of 0.52 +/- 0.05 $\mu m^2/s$.

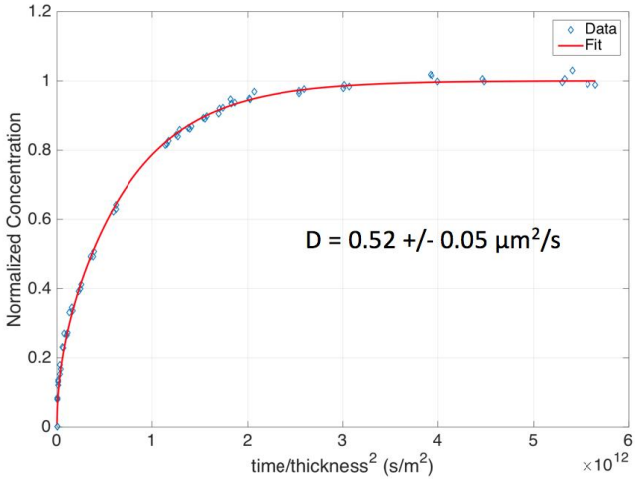

Figure 2. Sample diffusion data. Concentration of acrylate monomer in the urethane matrix is monitored as a function of time and sample thickness and fit to an infinite plane sheet diffusion model with a single fit parameter.

The rate of polymerization of the acrylate monomer was measured at 365 nm for intensities ranging from 1 – 20 mW/cm^2 using a Fourier Transform Infrared Spectrometer, as shown in Figure 3. Conversion of the monomer occurs over much faster time scales than the diffusion of monomer for all but the smallest of spatial scales.

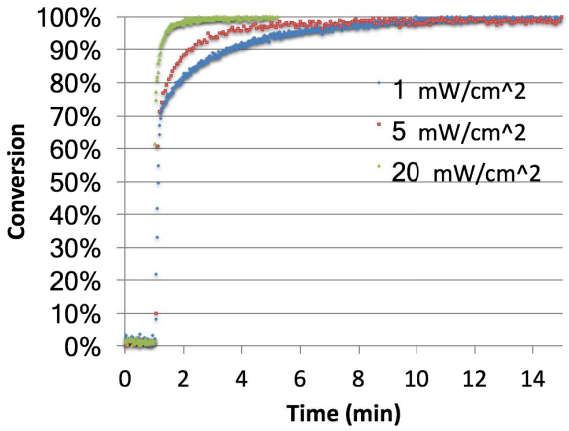

Figure 3. Fourier Transform Infrared Spectroscopy data on the conversion of acrylate monomer over time for three representative intensities at 365 nm.

Finally, through bulk shrinkage measurements, samples with 20 wt% writing monomer were found to have 2% shrinkage. This has not yet been incorporated into the mechanical model and will be in the future to refine the accuracy of the predictions. For the experiments reported in this work, swelling from diffusion of monomer has a much more significant effect on the deformation and bending of the material.

3. MECHANICAL MODEL

A multi-phasic mixture formulation [10,11] is used to describe the interactions between the base urethane matrix and the acrylate monomer during and after photo-polymerization along with the evolution of mechanical behavior of the composite. The mixture is composed of fluid-like constituents, such as the free monomer, which are crucial for chemical reactivity, and solid-like constituents, such as the base matrix and polymerized monomer. Both components undergo mass transfer, the former via diffusion and the latter via swelling. Additionally, it is assumed that the mixture is continuous for modelling. To describe the changing internal distribution of monomer mass, reaction-diffusion equations coupled with force equilibrium of the mixture are introduced in the following section.

3.1 Mass Transport

In a system with species of multiple phases, the solid constituents are typically described by a single displacement function $\boldsymbol{u}(\boldsymbol{X},\boldsymbol{t})$ for a given reference location $\boldsymbol{X}$. Using a constrained mixture formulation [12], the mass transfer of the fluid-like constituents is described in terms of the relative velocities with respect to the solid constituents. If all the constituents are assumed to be incompressible, the continuity equation [13] is given by

$$\nabla \cdot \boldsymbol{v} + \nabla \cdot (\phi_m \widetilde{\boldsymbol{v_m}}) = 0 \tag{1}$$

where $\boldsymbol{v} = \dot{\boldsymbol{u}}$ is the velocity vector of the solid constituents, ϕ_m is the volume fraction of fluid-like free monomers and $\widetilde{\boldsymbol{v_m}} = \boldsymbol{v}_m - \boldsymbol{v}$ is the relative velocity of free monomers with respect to the solid constituents. The term $\nabla \cdot \boldsymbol{v}$ is interpreted as the rate of volumetric swelling of the solid components. The relative velocity is written in terms of the Fickian diffusivity constant and the spatial gradient in the chemical potential [14] as

$$\widetilde{\boldsymbol{v_m}} = -\frac{D_m \nu_m}{RT} \nabla(\Delta\mu_m) \tag{2}$$

where D_m is the diffusion constant of the free monomers through the base polymer matrix, ν_m is the monomer molar volume, R is the gas constant, T is the temperature and $\Delta\mu_m$ is the chemical potential per unit volume derived from the Gibbs free energy for mixtures given by Flory [15] as

$$\Delta\mu_m = \frac{\partial \Delta G^{mix}}{\partial \phi_m} = \frac{RT}{\nu_m}\left(\ln\phi_m + (1-\phi_m)\left(1-\frac{\nu_m}{\nu_p}\right) + \chi(1-\phi_m)^2\right) \tag{3}$$

where ν_p is the molar volume of the solute, i.e. the base matrix in this case, and χ is the Flory-Huggins parameter which describes the polymer fluid interaction. Mass balance of the polymerized solid monomer is given by

$$\frac{d\widetilde{c_m}}{dt} = k_m(I,\boldsymbol{x})\, c_m \left(1 - \frac{\widetilde{c_m}}{\widetilde{c_m}^0}\right) \tag{4}$$

where c_m is the concentration of the fluid-like monomer, $\widetilde{c_m}$ is the concentration of the polymerized solid-like monomer network, $\widetilde{c_m}^0$ is the maximum concentration of solid monomers corresponding to complete polymerization and k_m is the polymerization rate constant which is a function of the light intensity I and spatial location $\boldsymbol{x}$. The value of k_m is obtained from experimental measurements by fitting the solution of the above equation to observed measurements as shown in Figure 4.

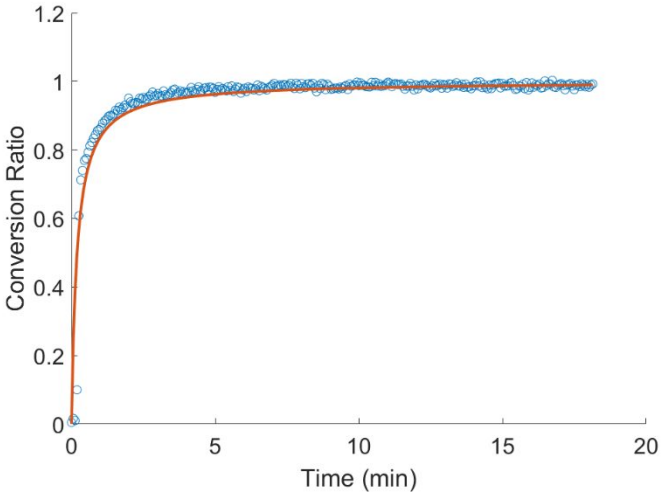

Figure 4. Plot of monomer conversion ratio with exposure time from experiments and fit with the solution corresponding to $k_m = 2.59\ /min$ for light intensity 5 mW/cm^2.

In addition to the above equations governing the mass transport of fluid constituents and rate of formation of solid constituents, a continuity constraint is imposed such that

$$\frac{1}{J} + \phi_m + \widetilde{\phi_m} = 1 \tag{5}$$

where J is the ratio of the current volume of the mixture (including swelling and mechanical deformations) to the dry volume of the matrix, and $\widetilde{\phi_m}$ is the volume fraction of the solid-like polymerized monomer. Thus, the overall distribution of mass of different components of the system is obtained by solving the above equations. It is to be noted that the mass distribution is governed by the competition between the polymerization rate and the diffusivity of the monomers.

3.2 Mechanical behavior

The mechanical or elastic properties of polymers are typically described using hyper-elastic models also called rubber elasticity. The base polymer matrix and newly formed polymerized monomer form interpenetrating networks. For both solid polymer networks, the Arruda-Boyce [16] model is used as the constitutive model for which the stress-strain relationship is given by

$$\boldsymbol{\sigma} = -p\mathbf{1} + 2C_1\left[\sum_{i=1}^{5} i\alpha_i\beta^{i-1}I_1^{i-1}\right](2\boldsymbol{\epsilon} + \mathbf{1}) \tag{6}$$

where $\boldsymbol{\sigma}$ is the stress tensor, p is the hydrostatic pressure due to incompressibility, $\boldsymbol{\epsilon} = \mathbf{1/2}(\boldsymbol{FF}^T - \mathbf{1})$ is the nonlinear strain given in terms of the deformation gradient $\boldsymbol{F} = \mathbf{1} + \partial\boldsymbol{u}/\partial\boldsymbol{x}$ for the macroscopic solid displacement field $\boldsymbol{u}(\boldsymbol{x}, t)$, $I_1 = tr(\boldsymbol{FF}^T)$ is an invariant, and C_1 and β are the material parameters. The values of α_i can be found in other references [17]. The parameter β is dimensionless and is interpreted as the limiting network stretch. C_1 has the dimensions of stress and is typically written in terms of the cross-link density of the polymer as $C_1 = \rho_x RT$, where ρ_x is the number of moles of cross-links per unit volume of the solute. We adopt this description for the base polymer matrix and the value of C_1 and β were obtained from experimental uniaxial compression tests as shown in Figure 5.

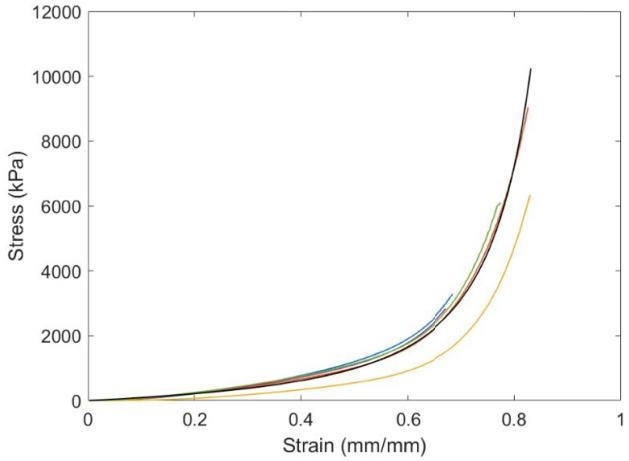

Figure 5. Plot of compressive stress vs strain for different samples of base matrix formed with 20 wt% monomer. The samples were unexposed to light. The black curve represents the model fit corresponding to $C_1 = 249.45, \beta = 0.0192$.

The additive mixture rule is used to describe the mechanical behavior of the entire material such that $\boldsymbol{\sigma} = \boldsymbol{\sigma}_p + \boldsymbol{\sigma}_m$, where $\boldsymbol{\sigma}_p$ is the stress due to the base polymer matrix and $\boldsymbol{\sigma}_m$ is the stress due to the newly formed solid monomer network. Compression tests with samples made from base polymer matrix with 20% wt monomer that are completely polymerized after light exposure are used to determine the material parameters of the solid monomer network. To account for the effect of changing solid monomer concentration, $\widetilde{c_m}$, due to polymerization on the mechanical property of the mixture, it was assumed that $\rho_x \propto \widetilde{c_m}$ for the solid monomer network. For 20 wt% initial monomer present in the matrix the concentration $\widetilde{c_m}$ after exposure to light was determined as 0.392 mol/L. The values of the material parameters were determined from the compression stress-strain plots as shown in Figure 6.

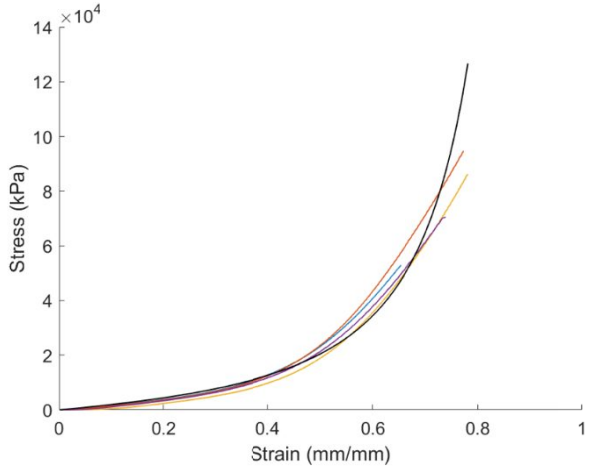

Figure 6. Plot of compressive stress vs strain for different samples of base matrix soaked in 20 wt% monomer and fully polymerized. The black curve represents the model fit corresponding to C_1=5022.24, β=0.0403.

4. LARGE SCALE DEFORMATIONS: BENDING OF FILMS

As a demonstration of the magnitude of the effect of the stress in the material caused by diffusion of the mobile acrylate monomer, large scale bending experiments are performed. The polymer formulation described above is set into 120 μm films and cut into strips that are ~ 3 mm x 8 mm. An optical absorber is added to create an intensity profile that

decreases in depth due to Beer-Lambert exponential absorption. Figure 7 (left) shows the process under which the polymer films bend. A uniform UV exposure on one side of the thin film results in a gradient light exposure in depth. The fractional transmission through the sample is shown in Figure *7* (right). The light initiates photopolymerization in the bright areas, causing an initial shrinkage and bending of the film toward the light. The monomer concentration gradient results in diffusion of monomer from the dark areas to the bright areas, causing swelling. The swelling results in bending of the film away from the light.

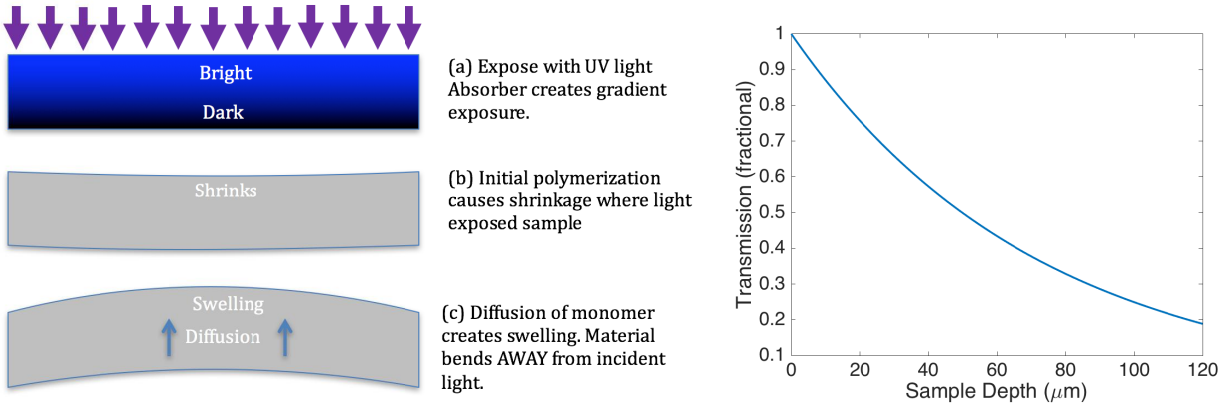

Figure 7. Process of self-folding. (a) Thin film is exposed with uniform UV light creating an exponential intensity profile in depth in material. (b) Polymerization in the bright areas causes shrinkage, causing the sample to bend slightly toward the light. (c) Polymerization causes a monomer concentration gradient and over time, monomer from the unexposed areas diffuse into the polymerized areas, causing swelling. This results in the material bending away from the incident light.

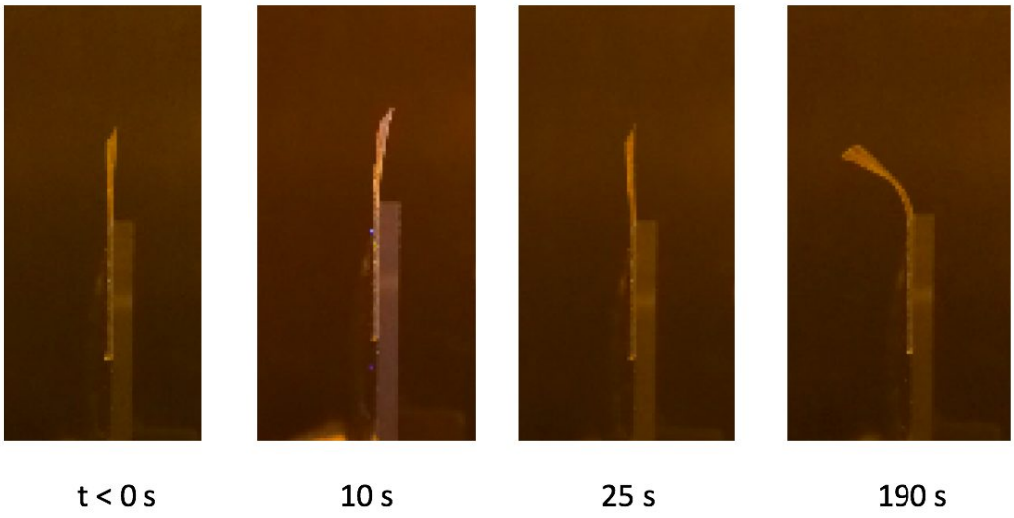

Figure 8. Time evolution of the bending of a thin film. The film is observed looking edge on. At t < 0 s, the 365 nm light source has not yet been turned out. 10 s after the light has been turned on, the film is observed to bend slightly toward the light due to shrinkage. After 25 seconds, swelling has bent the film back to its original position and after 190 s, significant bending away from the light source is observed.

Initial experiments with holographic photopolymers show a rapid initial shrinkage during illumination followed by a slower diffusion-mediated bending step, as shown in Figure 8. Full bending of 120 μm-thick films, with radii of curvature as small as 1 mm, is achieved in less than 2 hours with single optical exposure and no post processing. Figure 9 (left) shows a typical flat unexposed film alongside a similar circular film after exposure and full diffusion. Figure 9 (right) shows how control over the geometry of the sample can be used to control the final shape of the bent object. This work demonstrates the magnitude of deformations that are possible in these thin films using only diffusion of mobile monomer. It also illustrates how much more significant swelling is than shrinkage when diffusion is the dominant cause

of refractive index change. For example, an isolated exposure (e.g. a hologram) in a film of larger area will first tend to locally shrink but later, after sufficient time for monomer to diffuse from the film to the center of the exposure, swell due to the increased concentration of the mobile monomer.

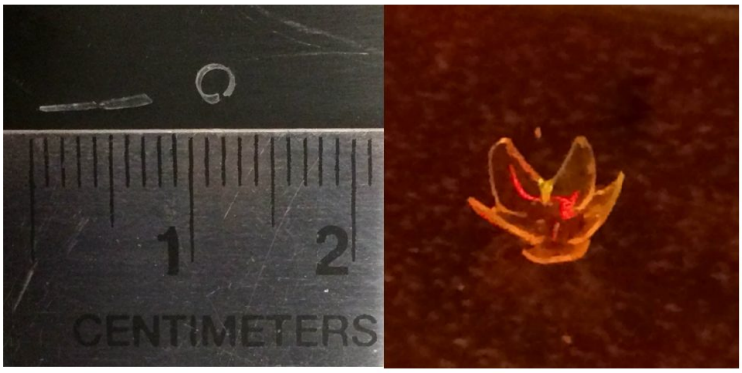

Figure 9. (Left) The left image shows a representative 120 μm film before (flat film on left) and after (circular film on right) exposure to UV light. (Right) The right image shows a similar film where the geometry of the film is used to control the bending.

5. SURFACE RELIEF GRATINGS

Surface relief gratings are an important consequence of diffusion of writing monomer in open or unconstrained films. Whether these gratings are a designed optical element or an undesired side effect, understanding more about their formation is essential when working with these diffusive photopolymers. In this paper, we explore the effect of the period of the grating on the surface height and qualitatively compare results from the model and experiment.

The surface gratings are written into the material by laminating a chrome on fused silica mask onto the surface of a 250 μm film and exposing the sample through the mask to 9 mW/cm^2 of 365 nm light from a UV lamp passed through a diffuser as shown in Figure 10. The mask is then removed and the samples are left to process for at least 24 hours, sufficient time to allow for complete diffusion of monomer from the dark to the light regions of the sample. These samples contain no absorber. The masks used are 50% duty cycle diffraction gratings with pitches of 20 μm, 40 μm, and 80 μm and the exposure time for each sample was 30 seconds.

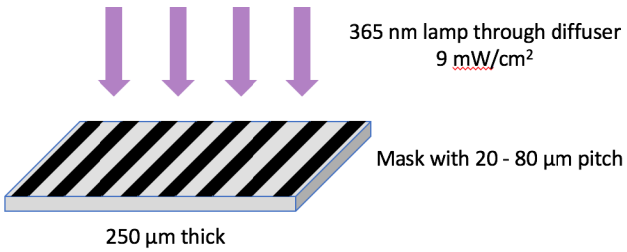

Figure 10. Schematic for writing surface relief gratings in photopolymer samples.

Once the monomer has had time to completely diffuse, the sample surfaces were evaluated using a scanning confocal reflection microscope as shown in Figure 11. A 660 nm laser is focused onto the sample using a 0.66 NA objective. The sample is scanned along the direction of propagation to find the front surface of the sample, then moved transversely and rescanned over 10 periods of each grating pitch. The data is averaged over three pitches to decrease the effect of noise in the measurement.

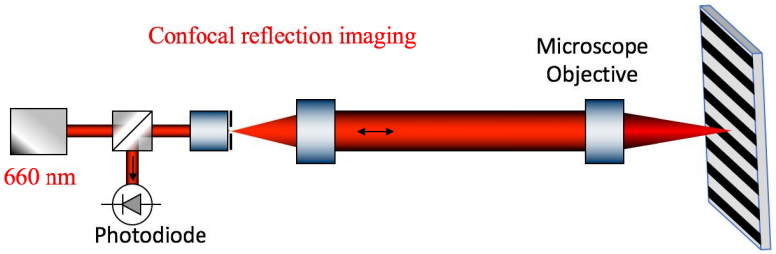

Figure 11. Confocal reflection microscope used to scan the front surface of the surface relief gratings.

For the surface gratings measured, the surface profiles are on the μm-scale in a 254 μm-thick sample, therefore reducing any boundary effects of the lower surface of the sample. The surface grating is written over the entire surface of a sample with transverse measurements of a cm^2. All surface measurements are made far away from the boundary of the sample, therefore considerably reducing any edge boundary effects, and so we conclude that the material can be modelled using periodic boundary conditions to good approximation. Based on the argument of periodicity, it is sufficient to model just one period of the square wave. When the problem is non-dimensionalized, one can see that different pitches do not change the relative widths of the high to low intensity regions. This leads to the conclusion that the surface profile solution is obtained from the model in the non-dimensionalized form and adjusted to get the value for different pitches. It follows that higher pitches will have proportionally higher surface deformations given that lighter regions swell and the darker regions shrink due to diffusion induced by polymerization. The resulting modeled surface profile is shown in Figure 12. Both axes are normalized by the period of the grating, so the figure shows one full period of the surface profile, and the peak to null surface deformation is approximately 1 x 10^{-2} times the pitch of the grating. The expected surface deformations for the samples under test is then 0.8 μm, 0.4 μm, and 0.2 μm for the 80 μm, 40 μm, and 20 μm pitch gratings respectively.

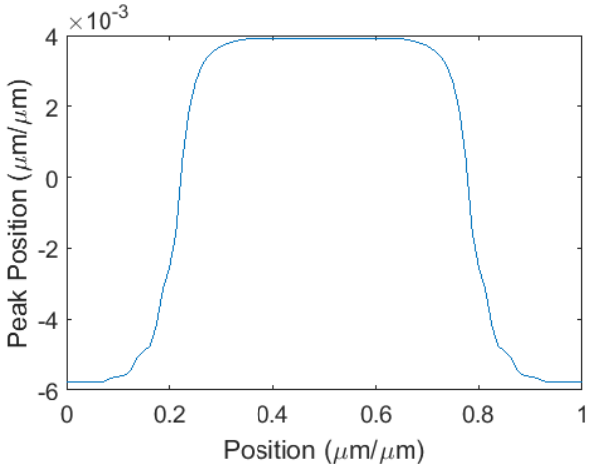

Figure 12. Plot of simulated surface profile normalized to the pitch length obtained from the model. Due to periodicity, only one pitch is simulated.

The experimental surface profiles for three gratings are shown in Figure 13. The *x*-axes are scaled to show three averaged periods of each grating, and the *y*-axes are constant to demonstrate the effect of the grating pitch on the surface height. As predicted by the model, the larger pitch gratings have a larger surface height. The average height of the surfaces are 3.6 μm, 2.2μm, and 1.1 μm with an uncertainty of 0.2 μm for the 80 μm, 40 μm, and 20 μm pitches respectively. While the model predicts a smaller surface grating by about a factor of 5, the qualitative trend is correctly predicted. The experimental gratings also have an additional surface bump in the dark regions that is not yet well understand, and may indicated additional dynamics that are not yet explained by the model.

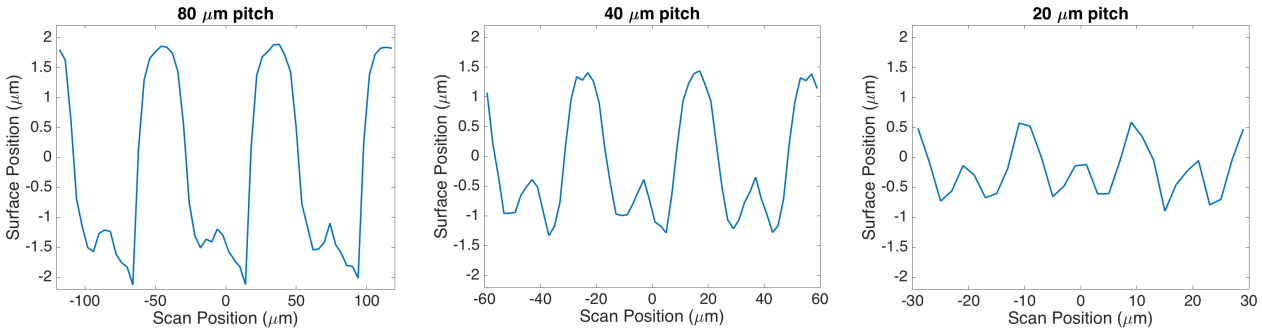

Figure 13. Surface profiles for three different pitch surface relief gratings written with identical writing intensities and times. The bright areas have a higher surface profile due to swelling of monomer into the polymerized regions. As the pitch increases, the surface height also increases.

This level of surface feature on an open film used for holography would diffract a significant amount of light away from the desired Bragg angle. We predict this linear trend of surface height with grating pitch will continue down to holographic pitches, on the order of 1 μm, where we would expect surface profiles on the order of 50 nm. The diffraction efficiency of such a surface profile is given by, η, of the q^{th} order of a thin sinusoidal grating [18],

$$\eta = J_q^2\left(\frac{m}{2}\right), \tag{7}$$

where J_q is a Bessel function of the first kind, order q, and m is the peak-to-peak excursion of the phase delay, in this case,

$$m = 2\pi\frac{(n-1)h}{\lambda}, \tag{8}$$

where n is the index of refraction of the polymer, h is the peak-to-valley height of the surface profile, and λ is the wavelength of the read light. For a surface profile of h = 50 nm, n = 1.5, and λ = 633 nm, this gives a first order diffraction efficiency η = 0.38%. Because the diffraction efficiencies add in field,

$$\eta = \left(\sqrt{\eta_{hologram}} + \sqrt{\eta_{surface}}\right)^2 = \eta_{hologram} + \eta_{surface} \pm 2\sqrt{\eta_{hologram}}\sqrt{\eta_{surface}}\,. \tag{9}$$

For a $\eta_{surface}$ = 0.38%, and a $\eta_{hologram}$ = 100%, this can result in a change in measured diffraction efficiency of 12%. Open or unconstrained films must therefore be carefully characterized and monitored to understand the effect of the surface relief gratings on the hologram performance for larger pitches.

On the other hand, when designing surface relief elements in these diffusive photopolymers, the dependence of the surface height on the feature size will have a significant effect on the processing. Smaller features will require larger exposure doses to result in equal surface heights as the larger features. Designing around this effect is essential to obtaining the desired surface features.

6. CONCLUSIONS

We have demonstrated an initial mechanical model for predicting the behavior of two-chemistry photopolymers used for holographic applications. We use standard chemical and mechanical materials measurements to calibrate the model. We demonstrate large scale bending of films in thin films. We also investigate the effect of grating pitch on the height of surface relief grating, with experimental results that agree with the linear trend predicted by the mechanical model. The experimental data demonstrates the magnitude of mechanical stresses that can be created in this model material and we demonstrate the large effect these small surface deformations can have on volume hologram performance. Further study of these mechanical deformations is essential for designing materials and optical exposures for manufacturing uniform, high diffraction efficiency holographic optical elements, and surface relief optical elements.

REFERENCES

[1] Marín-Sáez, J., Atencia, J., Chemisana, D., & Collados, M.-V. (2016). Characterization of volume holographic optical elements recorded in Bayfol HX photopolymer for solar photovoltaic applications. *Optics Express*, *24*(6), A720.

[2] G. Li, J.-A. Piao, M.-L. Piao, and N. Kim, "Full Color Holographic Optical Element Fabrication for Waveguide-type Head Mounted Display Using Photopolymer," J. Opt. Soc. Korea, Vol. 17, Issue 3, pp. 242-248 17, 242–248 (2013).

[3] Pandey, N., Naydenova, I., Martin, S., & Toal, V. (2008). Technique for characterization of dimensional changes in slanted holographic gratings by monitoring the angular selectivity profile. *Optics Letters*, *33*(17), 1981.

[4] Kawana, M., Takahashi, J., Guo, J., & Tomita, Y. (2015). Measurement of polymerization-shrinkage evolution during curing in photopolymer with a white-light Fabry-Pérot interferometer. *Optics Express*, *23*(12), 15356.

[5] K. Curtis, L. Dhar, A. Hill, W. Wilson, and M. Ayres, eds., Holographic Data Storage: From Theory to Practical Systems (John Wiley & Sons, Ltd, 2010).

[6] Colvin V, Larson R, Harris A and Schilling M1997 J. Appl. Phys. 81 5913–23

[7] Pavani, K., Naydenova, I., Martin, S., & Toal, V. (2007). Photoinduced surface relief studies in an acrylamide-based photopolymer. *Journal of Optics A: Pure and Applied Optics*, *9*(1), 43–48.

[8] Gallego, S., Márquez, A., Ortuño, M., Francés, J., Marini, S., Beléndez, A., & Pascual, I. (2011). Surface relief model for photopolymers without cover plating. *Optics Express*, *19*(11), 10896.

[9] Crank, J., [The Mathematics of Diffusion], Oxford University Press, London, 21-24 (1975).

[10] R. M. Bowen, Incompressible porous media models by use of the theory of mixtures, Int. J. Eng. Sci., 1980, 18(9), 1129–1148.

[11] M. A. Biot, Mechanics of Deformation and Acoustic Propagation in Porous Media, J. Appl. Phys., 1962, 33(4), 1482–1498.

[12] J. D. Humphrey and K. R. Rajagopal, A Constrained Mixture Model for Growth and Remodeling of Soft Tissues, Math. Models Methods Appl. Sci., 2002, 12(3), 407–430

[13] C. Li, R. I. Borja and R. A. Regueiro, Dynamics of porous media at finite strain, Comput. Methods Appl. Mech. Eng., 2004, 193, 3837–3870

[14] F. J. Vernerey, A mixture approach to investigate interstitial growth in engineering scaffolds, Biomech. Model. Mechanobiol., 2015, 1–20

[15] P. J. Flory, Principles of polymer chemistry, Cornell University Press, 1953.

[16] Arruda, E. M. and Boyce, M. C., 1993, A three-dimensional model for the large stretch behavior of rubber elastic materials, J. Mech. Phys. Solids, 41(2), pp. 389–412.

[17] Ateshian, G. A. & Ricken, T. Multigenerational interstitial growth of biological tissues. Biomech. Model. Mechanobiol. 9, 689–702 (2010).

[18] Goodman, J.W., [Introduction to Fourier Optics], McGraw Hill, Boston, 81-82 (1996).